University of Waterloo

PHYS460A

Nuclear Magnetic Resonance

Experiment #20

Authors:
Ben MacLellan
20510640

Michael Hamel
20519421

Kayla Hardie
20538454

Waterloo, ON

Date Performed: November 13, 2017
Date Submitted: November 27, 2017

Abstract

Nuclear magnetic resonance (NMR) arises from an intrinsic property of nuclei called spin. This property can be used to determine the molecular structure and purity of various samples. In this report, NMR is used to investigate the properties of various samples and to determine the the spin-spin relaxation times (T_2 and T_2^*) and spin-lattice relaxation (T_1) times. The samples explored are copper-sulphate doped water as a calibration sample, ethanol, and rubber. Free induction decay, inversion recovery, saturation recovery and Hahn spin echo techniques are used to determine the time constants. Ethanol is found to have time constants of $T_1 = 2357 \pm 82$ ms and $T_2 = 42.41 \pm 3.38$ ms, and rubber has $T_1 = 38.48 \pm 2.09$ ms and $T_2 = 4.80 \pm 1.11$ ms. These results demonstrate that for our samples, T_1 is approximately an order of magnitude larger than T_2, and the time constants for ethanol are an order of magnitude larger than that of rubber.

1 Introduction

Nuclear magnetic resonance (NMR) is the phenomena describing how the nuclei in a static magnetic field interacts with external effects, such as an applied magnetic field. This interaction is shown in the absorption and emission of radiation at characteristic rates. This phenomena is fundamental and is relatively simple – to the degree that it can be derived from the fundamental principles of quantum mechanics. Since this phenomena is fundamental and universal, it appears in several contexts and is of use to many different fields. As a result, the term NMR can mean different things to different people. One such use is MRI, originally named NMR imaging, which is arguably the most ubiquitous and widespread usage of "quantum technology". However, the context which we will be investigating it a more common lab experiment known as NMR pulse spectroscopy.

NMR generally involves applying a strong magnetic field to align nuclear magnetic moments under study, then a perpendicular magnetic field is applied to perturb this overall magnetic alignment. The study of the recovery to alignment can reveal details of the material under study. In pulse NMR spectroscopy this perpendicular magnetic field is applied for a specific amount of time to "push" the overall magnetic moment of the material into a known orientation, and then the perpendicular field is turned off and the recovery process of the material is observed to glean details of the material under study.

In this experiment three different pulse schemes are applied to three different materials to study their different recoveries and from this we can investigate the different materials and the different schemes used to make them. These materials are a calibration sample (doped water), ethanol, and rubber. The experiment also includes an investigation of the frozen doped water.

2 Theoretical Background

2.1 Resonance Condition: Larmor Frequency

By starting out and modelling a simple particle in a static magnetic field ($\vec{B_o}$) we can represent the Hamiltonian as: $H_o = -\vec{\mu} \cdot \vec{B_o}$, where we define the magnetic moment as $\mu = g\frac{q}{2m}\vec{S}$. Here q is charge, m is mass, and g as a proportionality constant (known as the g-factor). For any particle the q and m ratio will be unique, so we label this unique, identifying ratio the gyromagnetic ratio, $\gamma = g\frac{q}{2m}$.

Choosing the static field to be in the $\hat{z}$ axis, we can now state that:

$$\begin{aligned} H_o &= -\gamma \vec{S}\vec{B_o} \\ &= -\gamma \vec{S_z} B_o \end{aligned} \tag{1}$$

The S_z component for the spin $\frac{1}{2}$ (proton/electron) is defined as: $S_z = |\uparrow\rangle\langle\uparrow| - |\downarrow\rangle\langle\downarrow|$. Solving this Hamiltonian, gives us two possible energy eigenvalues which correspond to two possible states of spin up ($\uparrow$) and spin down ($\downarrow$). Hence we will label the allowed energies as $E_\uparrow$ and $E_\downarrow$.

$$E_\uparrow = -\gamma\frac{\hbar}{2}B_o \qquad\qquad E_\downarrow = \gamma\frac{\hbar}{2}B_o \tag{2}$$

This means we can only have energy transitions of: $\Delta E = E_\downarrow - E_\uparrow$. Translating this to a frequency we can state this photon absorption/emission frequency is:

$$\begin{aligned} \omega &= \frac{\Delta E}{\hbar} \\ \omega &= \frac{E_\downarrow - E_\uparrow}{\hbar} \\ \omega &= \gamma B_o \end{aligned} \qquad \text{(Larmor frequency)}$$

We can also find the Larmor frequency classically by considering that if the particle is not aligned with our static magnetic field it will experience a torque defined as: $\vec{\tau} = \vec{\mu} \cdot \vec{B_o}$ which will lead to a procession about the axis of the static field. This frequency of procession is exactly ω, the Larmor frequency.

2.2 Perpendicular Magnetic Field: Rabi Oscillations

The Hamiltonian in the energy basis is :

$$H_o = E_\uparrow |\uparrow\rangle \langle\uparrow| + E_\downarrow |\downarrow\rangle \langle\downarrow| \tag{3}$$

Creating a potential to induce transitions in the xy-plane and calling this potential $\vec{B_1}$ and allowing it to rotate at the Larmor frequency gives us:

$$V(t) = -\vec{\mu} \cdot \vec{B_1}$$
$$V(t) = \gamma B_1 \frac{\hbar}{2}\big(e^{-i\omega t} |\uparrow\rangle \langle\uparrow| + e^{i\omega t} |\downarrow\rangle \langle\downarrow|\big)$$

We now note that generally we can prove working in the Dirac Interaction picture gives:

$$i\hbar\frac{\partial}{\partial t} |\psi(t)\rangle = V(t) |\psi(t)\rangle$$

$$|\psi(t)\rangle = \sum_n c_n |n\rangle$$
$$H_o |n\rangle = E_n |n\rangle$$

Combining the above three equations we have that:

$$i\hbar\frac{\partial}{\partial t} c_n(t) = \sum_m c_m V_{nm}(t) e^{i\omega_{nm} t}$$

We note that ω_{nm} is the transition frequency which, for our originally stated particle, is the Larmor frequency. We also note that plugging in our stated potential (Equation 1) gives us a single solution for $c_\uparrow$ and $c_\downarrow$ which is: $c_\uparrow = c_\downarrow = \sqrt{1/2} \cdot c^{i\gamma B_1}$. So, the atoms will transition between $|\uparrow\rangle$ and $|\downarrow\rangle$ at a frequency of:

$$\omega_R = \gamma\frac{B_1}{2} \qquad \text{(Rabi frequency)}$$

This means that the additional magnetic field which is applied at the Larmor frequency will create an oscillation between the two states at a rate of the Rabi frequency.

2.3 Nuclear Magnetization

The bulk magnetic moment of a sample is the summation of magnetic moments, if we assume that the atoms have no orientation preference. Usually this discussed in the context of paramagnets, which are the summation of atomic-based electron distributions, but we note that this effect can also occur with nuclear magnetic moments as well. This summation of nuclear magnetic moments leads us to $\vec{M} = \vec{\mu}\,(C_\uparrow - C\downarrow)$, where $C_{\uparrow\downarrow}$ are the concentrations of up vs down spin states.

Due to the B_o static magnetic field we have an energy difference of $\Delta E = 2\mu B_o$ and hence the number of protons in the lower energy state ($\uparrow$) is slightly lesser leading to a measurably larger $C_\uparrow$ than $C_\downarrow$. This distribution is due to thermal effects.

2.4 Pulsed NMR

When a B_1 pulse for time τ is applied, the magnetization will be changed by an angle of $\theta = \omega_R \tau$. This is the azimuthial angle with the static electric field, as $\theta = 0$. This means that with a carefully timed pulse we can force the overall $\vec{M}$ from $+\hat{z}$ to any azimuthial angle.

We describe the pulses by the affect they cause on the direction of $\vec{M}$. Hence a pulse which brings $\vec{M}$ to the xy plane is described as a $\pi/2$ or 90° pulse, and a pulse which brings it to $-\hat{z}$ as a π or 180° pulse. Of course any angle being created is possible, but only $\pi/2$ or π pulses will be discussed.

2.5 Defining Time Constants

After the application of a $\pi/2$ pulse, $\vec{M}$ will process about the z-axis on the xy-plane at a rate of ω, the Larmor frequency. If a coil is placed around the sample the processing magnetization will produce a magnetic field, inducing a voltage within the wire (the same used to create the pulse) due to Faraday's Law. This will induce: $V(t) = V_o sin(\omega t)$ where $V_o = \omega k M_T$, M_T is defined as the magnetization component in the xy-plane, and k is a scaling factor of the coil based off of factors such as shape and size of the coil and other physically constant features. From this, we can note that $V_o \propto M_T$ as k and ω are constants of the experiment.

A typical signal suffers from decay, which can be modelled as $V(t) = V_o e^{-t/T} sin(\omega t)$. The exponential decay can be described with a constant T – which can be broken up into individual quantities arising from different physical effects. These effects occur in different axes and are therefore presented as T_2^* and T_1.

T_1 is the so called "spin lattice relaxation time" and this is an effect describing the amount of time it takes for the sample to reach thermal equilibrium. This return is only achieved in the direction of the static field as it is the spins returning to thermal equilibrium (a return to alignment with B_o). The decays can occur from any position, but solely add to the $+\hat{z}$ component.

T_2 is known as the "spin-spin relaxation time" and is defined as the amount of time it takes for the spins of a system to move out of phase with each other due to the local internal magnetic fields, which are produced by neighbouring spins. These are originally in phase due to the B_1 pulsed field forcing them to be at the same xy angle. Thus after a magnetization $\vec{M}$ is turned onto the xy plane, the spins begin to de-phase, decreasing the net $\vec{M}$ and decaying the signal.

This de-phasing can also occur due to inhomogonities in the applied static field, which always occur. This effect is noted as $\frac{1}{T_2^B}$, but can also be proven to be dominated by a linear term in a paramegnet based NMR which can be represented as: $\frac{1}{T_2^B} = \gamma \Delta B_o$, where the ΔB_o are the deviations of the static field from the perfect field. The term $1/T_2^*$ is commonly used to represent $1/T_2^* = 1/T_2 + 1/T_2^B$. These effects are logically grouped together as phase decoherence times only affect the magnetization in the xy-plane.

We also note that any Rabi shift of $\pi/2$ will cause these orthogonal components to interact with each other, and thermal decay can bring a xy aligned atom into the static field direction.

These effects all combine to give us a signal in the xy-plane of $V(t) = V_o e^{-t/T_2^*} sin(\omega t)$ as defined above. Which can be seen in Figure 1. We note that the envelope which the decay occurs in is called the "free induction decay" (FID).

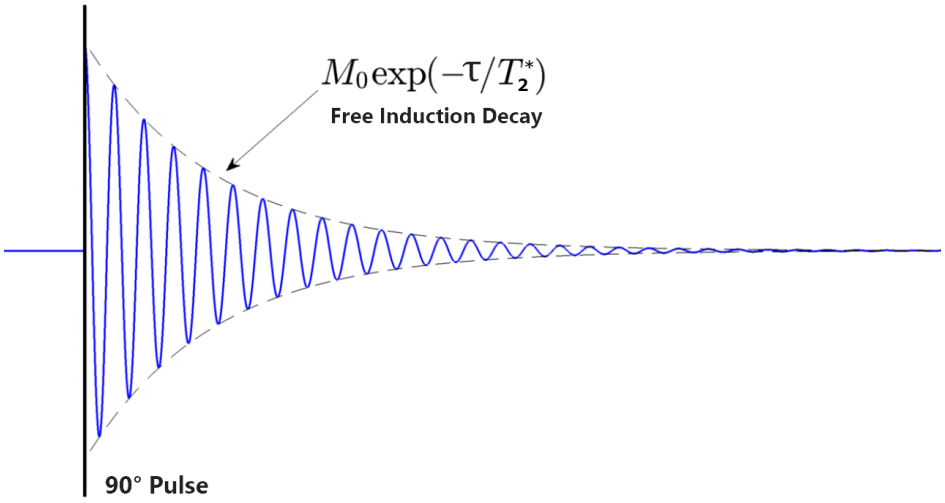

Figure 1: Showing the signal which should be received from a $\pi/2$ pulse in an idealized simulation of an actual experiment.

3 Experimental Background & Procedure

3.1 Apparatus

This lab is based around a single piece of equipment – the Nuclear Magnetic Resonance spectrometer. The particular spectrometer utilized for the following experiments is shown in Figure 2.

Figure 2: NMR spectrometer apparatus with labelled potentiometer dials, taken from the lab manual

The NMR spectrometer was developed in the 1950s and is commonly used to test atomic and molecular properties of samples. The spectrometers must be tuned to the particular atom which they are measuring – setting the coil's signal equivalent to the Larmor frequency of the atom to create a resonance condition (the coil is often called the radio frequency (RF) coil as most Lamour frequencies are in the RF range). Our particular NMR spectrometer is set at a fixed frequency of 9MHz to approximately match the proton's resonance with our particular permanent magnet, but due to environmental variations this resonance frequency must be adjusted. Hence an adjustment knob is available to give a fine adjustment to the RF signal inputted (±60kHz). This is adjusted with usage of knob #9.

It is possible to run many types of experiments as described in Sections 3.2.1, 3.2.2 & 3.2.3. These experiments can be chosen with the usage of knob #1.

There are two knobs labelled 90° and 180° which are simply potentimeters to adjust the length of the B_1 pulse, hence these potentimeters directly result in affecting the overall $\vec{M}$ orientation. We note that these "90° " and "180° " knobs do not necessarily create the angles which are printed on the device, but simply correlate to the 90° and 180° pulses in the respective chosen experiments.

The ability to adjust the length of time between the experiments is also crucial for many of the experiments, and this length can be adjusted manually with usage of knobs #7 & 8. We note that although there is a dial which gives us the time delay, this reading is not used, instead the time delay is calculated during the data analysis as this digital measure will be more accurate and uniform across the experiments.

The sample is placed in a vial and ensured to be in place at the point of highest magnetic field to give the largest contrast. Also the samples are "normalized" which in this context means that they are set to give roughly the same voltage signal even in substances with dramatically different proton density (for example: rubber). Hence the sample is "normalized" with respect to voltage. The sample is placed in the holder which is labelled as #10.

The left portion of the spectrometer allows for the changing of detection properties, however only the reference phase will be added to create a lock in detector to see the FID on the intrinsic $\sin(\omega t)$ signal which is known to exist from $V(t) = V_o e^{-t/T} sin(\omega t)$. This allows for the accurate detection of the envelope. This reference phase is adjusted through usage of knob #13 and is activated through switch #12. During the experiments, this value is always kept locked into phase sensitive detection.

A filter is also included in the device, however the parameters of this filter are left untouched. Instead, digital filtering is performed in post-processing data analysis. The use of this filter is discussed in Appendix A.

All other switches and knobs are unused for this experiment. The raw signal from the detection equipment is measured on an oscilloscope, and data sets are saved for post-processing analysis and as representative results.

3.2 Experimental Types

There are several types of experiments which can be completed with a NMR spectrometer, each of which depends on pushing the $\vec{M}$ into different orientations in succession. The first pulse prepares the initial magnetization, and the second pulse measures the overall magnetization change which has occurred after a waiting period, τ. It is important to note that only the voltage induced due to Faraday's Law is measured. This voltage is proportional to the magnetization in the xy-plane: ($V \propto M_T$). So, while decay equations and relationships will be stated with respect to the $\vec{M}$, measured quantities and experimental data is provided in terms of V.

The rate of magnetization decay on the xy plane is:

$$M(t) = \vec{M}_o e^{-t/T_2^*} \tag{4}$$

However, we note that the magnetization on the z-axis decays without the T_2 & T_2^B these effects only apply to the perpendicular components to B_o in a sustained field. Hence the decay is modelled as:

$$M(t) = \vec{M}_o - (\vec{M}_o - \vec{M(0)})e^{-t/T_1} \tag{5}$$

We will first look at two methods of measuring the T_1 quantity directly.

3.2.1 Inversion Recovery ($\pi \to \pi/2$)

The application of a 180° pulse, $M(\tau = 0) = -\vec{M}_o$. After waiting for a time τ, $M(\tau = \infty) = \vec{M}_o$. From Equation 5, we can state that:

$$\begin{aligned} M(\tau) &= M_o - (M_o + M_o)e^{-t/T_1} \\ &= M_o(1 - 2e^{-t/T_1}) \end{aligned} \tag{6}$$

During the inversion time τ (between the 180° and 90° pulses), the magnetization of the inverted sample regrows under spin lattice relaxation or thermal equilibrium toward the $+z$-direction. At the time of the 90° pulse, push all of the z-component is pushed into the xy-plane where it can then be read. Thus sometimes, the secondary pulse is known as a "read" pulse. We note that the $\pi/2$ degree pulse still result in a FID which decays primarily due to spin-spin relaxation, but only the FID's peak is graphed as this shows the z-state after time τ.

3.2.2 Saturation Recovery ($\pi/2 \to \pi/2$)

This scheme is similar to Inversion Recovery, but pushes the $\vec{M}$ to the xy plane instead of to $-\hat{z}$. This means: $M(\tau = 0) = 0$ and $M(\tau = \infty) = \vec{M}_o$. Therefore:

$$M(\tau) = M_o(1 - e^{-t/T_1}) \tag{7}$$

This scheme is useful in certain circumstances, such as if the signal cannot be inverted as is true for quadrupolar molecules. It also has lower settle times which can lead to shorter experiments.

Comparing Saturation Recovery and Inversion Recovery, the Inversion Recovery method has longer recovery times and hence, is more accurate. However, in clinical settings this may cause some issues due to longer wait times in scans, while the higher resolution is generally desirable in non-clinical settings.

3.2.3 Hahn/Spin Echo ($\pi/2 \rightarrow \pi$)

Initially a 90° pulse generates a transverse magnetization in the xy-plane and this component (which can be measured as voltage) goes as $M_T = M_o e^{\tau/T_2^*}$. Some dephasing will occur following this due to local field inhomogeneities. This dephasing is dependant on some spins processing quicker than others due to a higher local field at that location and leaving some other slower processing spins behind at the "back of the pack".

After a time τ, an inverting pulse (180°) is applied and the phases begin to dephase again. However, the regions of quicker processing spins will now be at the "back" and after a time 2τ, both the slower and quicker regions will once again rephase once they reach the initial location. This rephased signal is known as the *echo*.

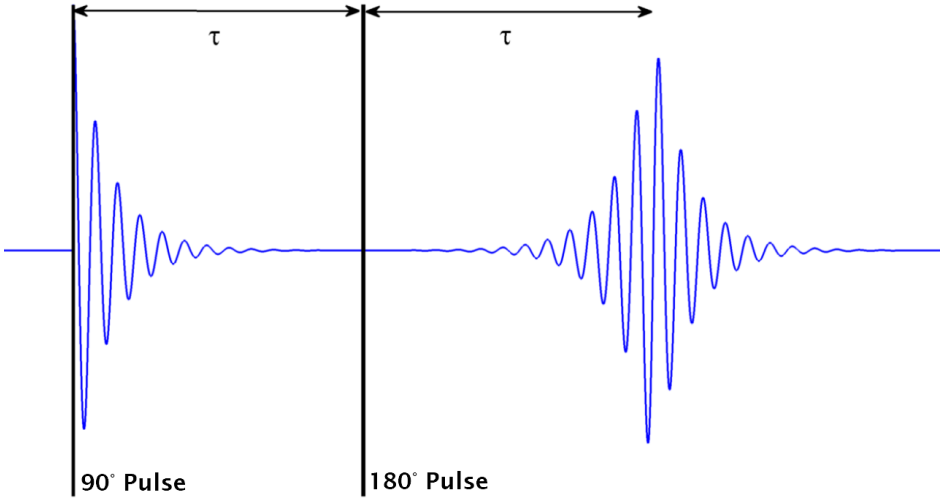

Figure 3: An idealized simulation of a Hahn spin echo experiment with no static field inhomogeneities.

However not all of the inhomogeneities can be reversed. For paramagnet based NMR spectrometers the static field inhomogeneities dominate relaxation and the samples dynamic fields (ex. water molecules move and may experience different forces because of their alignment difference) and these effects are non-symmetric about the inversion. This means that the rephased echo will be smaller by a factor of these static field inhomogeneities, which can be modelled as,

$$1/T_2^* = 1/T_2 + \gamma \Delta B_o \tag{8}$$

In principle this experiment does not need to be completed by an inverting pulse, and these general experiments are known as spin echo experiments. However the combination of 90° $\rightarrow$ 180° produces the maximal signal and this is known as the Hahn Echo [6].

3.3 Experimental Procedure

During the course of the investigation six different experiments are completed. They are:

1. Measurement of the Free Induction Decay (FID) of doped water at pulsed phases of $\frac{\pi}{2}$, π, $3\frac{\pi}{2}$ to observe the effects on the signal (Section 4.1).
2. Measurement of T_2^* by fitting the FID curve to doped water, ethanol and rubber, all using a single $\pi/2$ pulse (Section 4.2).
3. Usage of the Saturation Recovery Sequence (3.2.2) to find T_1 (Section 4.3). A rough measure is found, when $\mathrm{M}(\tau) = M_o/2$ which can be used to approximate T_1. Testing is completed on all three samples.
4. Use of Inversion Recovery Sequence (3.2.1) to find T_1 (Section 4.4). The decay of τ vs M_T is taken at many τ and the intersection/fit can be used to accurately find T_1. Testing is completed on all three samples.
5. Use of the Spin Echo Experiment (3.2.3)) to approximate the T_2^B term and remove it to find an accurate measure for T_2 (Section 4.5). Testing is completed on all three samples.
6. Analysis of frozen (solid) doped water to explore the effects of freezing has on the FID (Section 4.6).

3.3.1 Finding Desired Recovery Time

Finding the secondary pulse's recovery time is a non-trivial exercise. The following procedure describes how to calibrate the recovery times for the two pulse system.

1. On settings for free induction decay (FID) experiment, adjust the repetition rate, detector phase, and first pulse length to maximize the signal for a 90 degree pulse.
2. Measure the peak magnetization M_0, directly following the pulse.
3. Switch to inversion recovery (IR) experiment.
4. On the oscilloscope, two peaks are visible – corresponding to the two pulses. Reduce the time delay between them and maximize the first pulse (180 degrees) such that the first peak is approximately zero and the second is maximally negative. At this point the pulse sequence is 180-τ-90.
5. If the desired pulse sequence is 180-τ-90, then the parameters are set and the data can be collected (Section 4.4). However, if the desired sequence is 90-τ-90 (Section 4.3) then approximately halve the value of the first pulse's potentiometer.

3.4 Data Analysis

All data post-processing was completed using custom Matlab (Mathworks Ltd.) scripts, which are available at `https://github.com/tokiyoshi/460_E20_NMR.git`, along with all raw data and figures. All data was zero-shifted (such that the background is equal to zero) prior to further processing. In addition, the initial detector peak was removed from all data. This peak is caused by a ringing in the detector circuit. Filtering was performed (if needed) using a Gaussian smoothing algorithm with varying window size. Filtering was only performed if a peak value was to be automatically detected. See Appendix A for discussion on data smoothing.

4 Analysis

4.1 Finding Resonance

To begin, the NMR spectrometer settings were adjusted explore how they impact an FID signal for the doped water sample. Adjusting the repetition time had no measurable impact on the signal, indicating that water spin-lattice relaxation (regrowth) time is less than (or equal to) the lowest repetition time setting of 0.3 seconds. The receiver gain was not adjusted as increasing it reduced the signal-to-noise ratio of the spectrometer. The receiver phase and the 90 degree pulse dial were adjusted to maximize the signal. Adjusting the 90 degree pulse dial adjusts the amount of time that the sample experiences the applied magnetic field, B_1. In our system, the magnetization vector, $\vec{M}$, begins pointing in the direction of B_0, which is defined as the z-direction. The B_1 field is applied in such a way that it rotates the $\vec{M}$ vector into the desired orientation. A 90 degree pulse, as shown in Figure 4, occurs when the B_1 field has been applied until $\vec{M}$ points along the xy-axis. As our detection system is designed to measure the magnetization along the x-axis, the signal is maximized for this type of pulse.

Similarly, for a 180 degree pulse M is pointing in the negative z-direction and the signal is reduced to approximately zero. For a 270 degree pulse, the signal is minimized (negative peak) as it is pointing along the negative x direction.

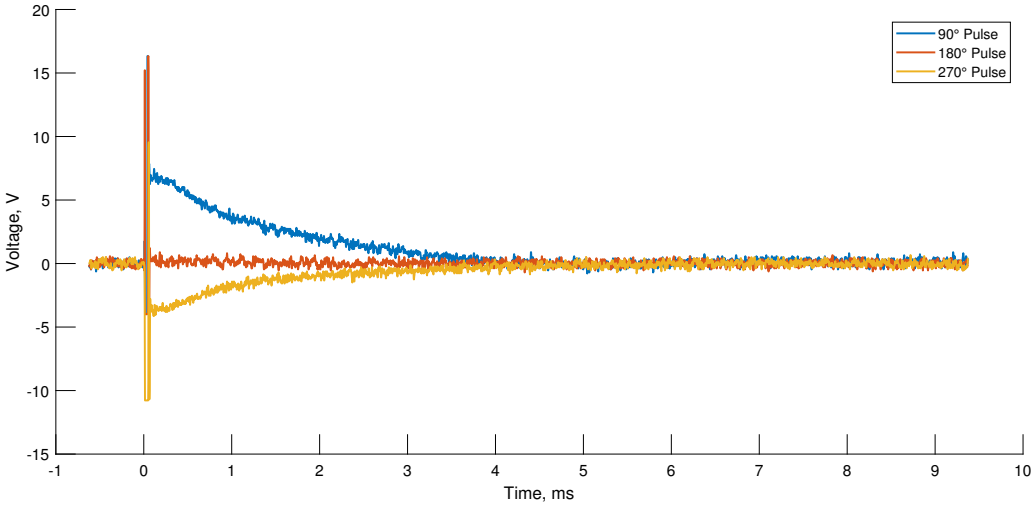

Figure 4: FID of doped water for a 90, 180 and 270 degree pulses.

4.2 Finding T_2^* for Water, Ethanol and Rubber

Similar to Section 4.1, the FID of three samples (doped water, ethanol, and rubber) were measured for 90 degree pulses only. The repetition rate, detector phase, and pulse value were set to maximize the signal for each sample.

The magnetization as a function of time for the FID experiment is given by the expression,

$$M_y(t) = M_0 e^{-t/T_2^*} \tag{9}$$

Taking the natural logarithm of both sides of this expression,

$$\ln(M_y(t)) = -t/T_2^* + \ln(M_0) \tag{10}$$

The first method to calculate T_2^* is an approximation method. From Equation 9, when $t = T_2^*$ the magnetization is $M_y = M_0/e$; thus by calculating the time where the magnetization has decayed to this value is an approximate value of T_2^*. From the FID of each sample, the peak magnetization M_0 is measured and the intersection of the decay slope with M_0/e is calculated. This is demonstrated in Figure 5 for doped water, and the estimated values of T_2^* are summarized in Table 1 (see Figure 14 in Appendix for T_2^* estimation plots for ethanol and rubber). The uncertainty values in our estimated time constant are taken as the uncertainty in determining M_0. This method is highly inaccurate, and is used only as an initial estimation.

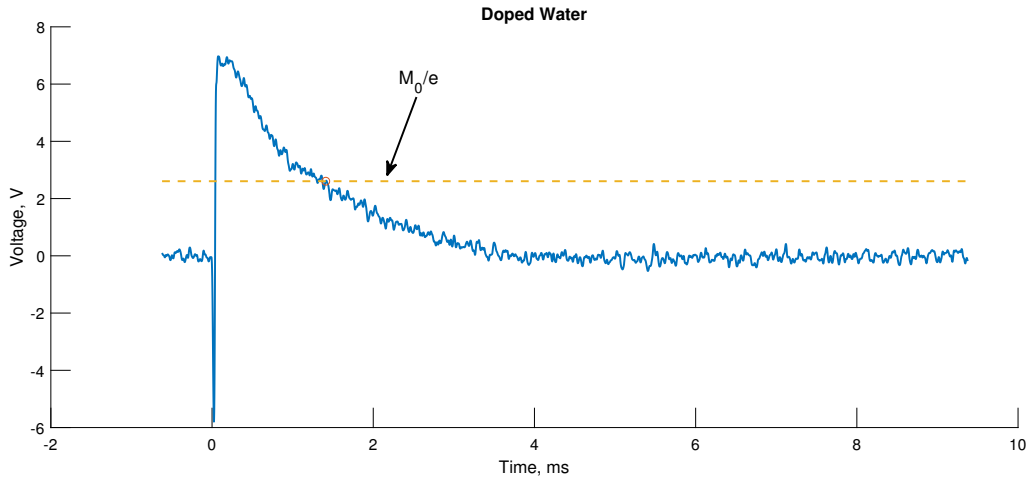

Figure 5: Estimation of T_2^* for doped water using the time value where $M_y \approx M_0/e$. Values for other samples are tabulated in Table 1.

A more accurate method of calculating the time constant T_2^* is to use a linear fit with the form of Equation 10. Prior to fitting, each data set was zero shifted; and no filtering was performed for these data sets. The natural logarithm of the magnetization was fit with a linear slope using the method of least squares. Only the portion of the data set which contained a strong signal was used in the fitting process, as the signal to noise ratio with the rest of the data set is too low to generate an accurate value of T_2^*. The uncertainty in these measurements are regarded as the 95% confidence interval of the fitting algorithm. Figure 6 demonstrates the fits for each sample (note that this plot demonstrates the fit data converted back to exponential form, to demonstrate the accuracy of the fit to the raw data).

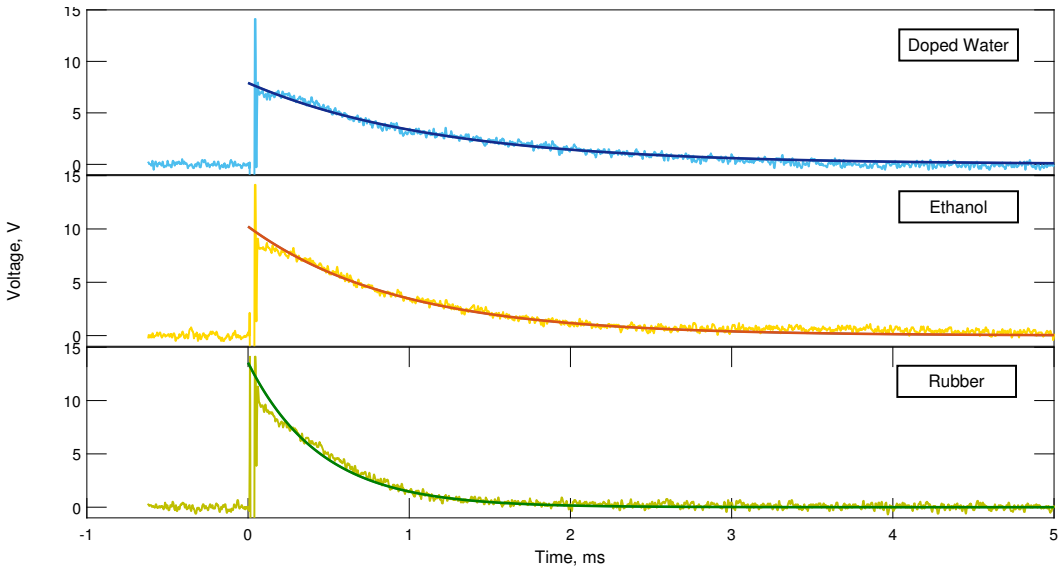

Figure 6: FID from a 90 degree pulse for doped water, ethanol, and rubber to determine T_2^*.

The behaviour of each fit matches quite well with the experimental data, following the trend very closely. The R^2 values in Table 1 are based off of the linear fit to the natural logarithm (see Figure 13 in the Appendix).

For each sample, directly following the pulse there is a reduction in the peak value from what the theoretical model predicts. This is likely caused by cross-talk effects between the applied pulse and detector – which is a systematic instrument error and could be reduced by readjusting the spectrometer settings. It could also be that there may be a better method to remove the detector peak.

Sample	T_2^* Estimate	T_2^* (ms)	R^2	Percent Difference (%)
Doped Water	1.4110 ± 0.1472	1.169 ± 0.017	0.9324	18.76
Ethanol	1.2270 ± 0.1472	0.9239 ± 0.0085	0.9638	28.18
Rubber	0.6415 ± 0.1104	0.4495 ± 0.0073	0.9550	35.20

Table 1: Summarized values of T_2^* for the three samples. First column is calculated using th estimation of $M_y = M_0/e$, depicted in Figure 5. The second column is calculated from the fits depicted in Figure 6, with the corresponding R^2 goodness-of-fit value.

Comparing the two methods summarized in Table 1, we see that the estimated value of T_2^* is always greater than the calculation using a fit.

4.3 Finding T_1 for Water, Ethanol and Rubber Using Saturation Recovery Sequence

With a 90°-τ-90° pulse sequence, the magnetic vector regrowth along the z-axis is given by equation 7,

$$M_z(t) = M_0(1 - e^{-\tau/T_1})$$

As the second pulse has been set to have $M_z = M_0/2$,

$$\frac{1}{2} = 1 - e^{-\frac{\tau}{T_1}}$$

Taking the natural logarithm of both sides and rearranging,

$$T_1 = \frac{\tau}{\ln 2} \tag{11}$$

The time delay between the two pulses, τ, was measured in post-processing by calculating the peaks in of the digital oscilloscope trace data. τ was set such that,

$$M_z \approx M_0/2 \tag{12}$$

As the determination of what time delay τ satisfies Equation 12 is approximate at best, three data traces were saved and analyzed in post-processing. The three data sets spanned the approximate range of time delays, such that the data sets have peak magnetization of $\lesssim M_0/2$, $\approx M_0/2$ and $\gtrsim M_0/2$. A simple 90° FID (as in Section 4.1) was used to calculate a $M_0/2$ in post-processing. A linear slope was fit between the time-delayed peaks of the three approximate data sets (see Figure 7) and the point on this slope where $M_z = M_0/2$ is our calculated value of τ. T_1 is then computed using Equation 11. As there is a large number of error in this measurement caused by uncertainty in the measurement of M_0, the peak detection on the saturation recovery peaks, and the linear fit, the uncertainty is taken to encompass the recovery peaks in all three traces. It could be an improvement to take more than three data points to create the line but this is a rough approximation so additional data points were not taken.

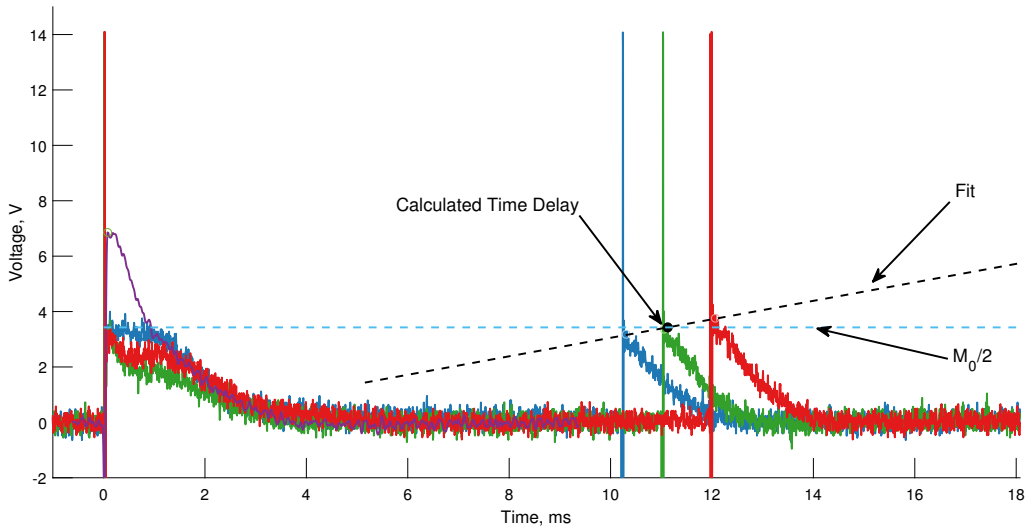

Figure 7: Three doped water saturation recovery traces with $\tau \approx M_0/2$, as well as 90 degree FID (purple trace) to measure M_0 with greater precision. Calculated τ value is shown as black circle and linear fit is dotted black line.

This process was repeated for ethanol and rubber, and the calculated T_1 values are tabulated in Table 2.

Sample	T_1 (ms)
Doped Water	16.2770 ± 1.1537
Ethanol	1029.1 ± 80.1
Rubber	34.1179 ± 5.658

Table 2: T_1 values for three samples, measured using a saturation recovery pulse sequence.

A second method for estimating T_1 can be performed during this experiment. While probing the sample with a 90° FID sequence, the signal will decrease rapidly when the repetition rate is approximately equal to $5T_1$. By reducing the pulse repetition rate until no signal is visible, the previous repetition rate is a highly approximated value of $5T_1$. This estimation of T_1 is highly imprecise as there is only 5 options for pulse repetition rate with large space between them. Thus, the 'resolution' of this method is very low. The calculated time constant would always be greater than its true value, as the last setting *prior* to the signal decrease is used as the estimate. This method was not performed, but could be useful for gaining insight into the order of magnitude and an upper bound for T_1.

4.4 Measuring T_1 for Water, Alcohol and Rubber Using the Inversion Recovery Sequence

An inversion recovery (IR) protocol was performed on the three samples using a 180-τ-90 pulse sequence and all parameters set to maximize the signal. This method is called inversion recovery as the magnetization is initially *inverted* to the negative z-direction. As it *recovers* to the positive z-direction, the second 90° pulse knocks whatever total magnetization is in the z direction to the xy-plane – essentially probing what amount the magnetization has recovered in the time τ.

The magnetization at the time-delay of τ is given by equation 6,

$$M_z(\tau) = M_0(1 - 2e^{-\tau/T_1})$$

Rearranging and taking the natural logarithm of both sides,

$$-\frac{\tau}{T_1} = \ln\left(\frac{1}{2} - \frac{M_z(\tau)}{2M_0}\right) \tag{13}$$

Each data trace was zero-shifted and filtered using a Gaussian filter (discussed in Appendix A), followed by a simple peak detection to determine the time-delay τ and the peak magnetization $M_z(\tau)$ (see Figure 8). The initial magnetization, M_0, was recorded as the maximum of a single FID for each sample (see, for example, Figure 4). These values were extracted from each experiment and compiled in Figure 9. Using Equation 13 to fit the data to linear slope we calculate T_1 for each sample, which are tabulated in Table 3.

The T_1 values for each sample can also be calculated using the zero-crossing (ZC) method. From Equation 13 with $M_z(t) = 0$,

$$T_1 = \frac{\tau}{\ln(2)} \tag{14}$$

So, using the above equation with a rough estimate of the value for τ where $M_z(\tau) = 0$ we can generate a rough guess of T_1.

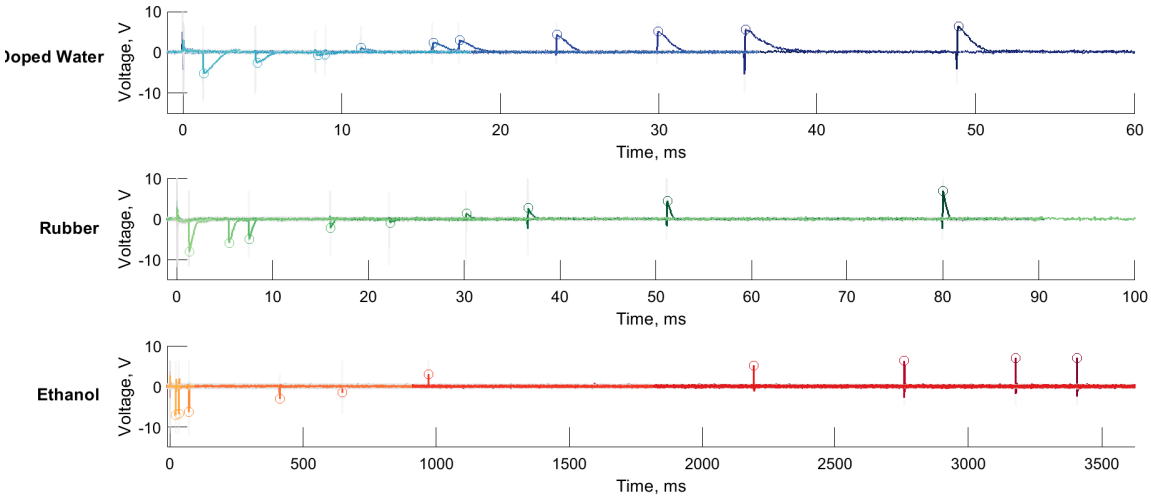

Figure 8: Oscilloscope traces of IR sequence for three samples after zero-shifting and filtering to determine peak magnetization values for each value of τ. Solid lines are the filtered data, light gray lines represent the raw, unfiltered data, and circles represent the computed peak magnetization values at τ.

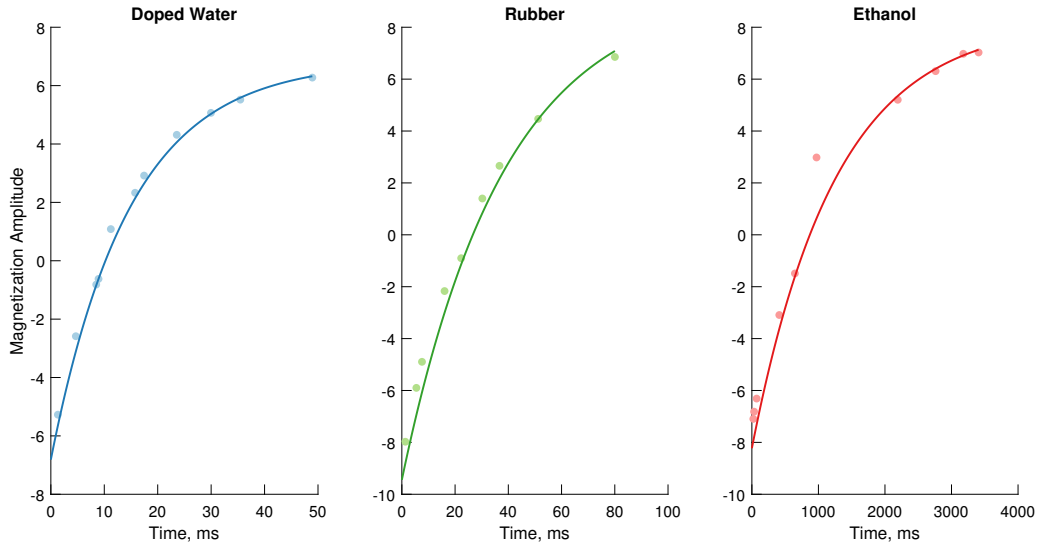

Figure 9: Peak magnetization values at a time-delay of τ (coloured circles) with the corresponding fit (solid line), calculated from the traces demonstrated in Figure 8 for doped water, ethanol and rubber.

Sample	IR Method T_1 (ms)	ZC Method T_1 (ms)	Percent Difference (%)
Doped Water	14.74 ± 0.41	14.0 ± 1.2	5.15
Ethanol	1257 ± 82	1117 ± 168	11.79
Rubber	38.48 ± 2.09	37.2 ± 3.1	3.38

Table 3: T_1 values for three samples calculated using the inversion-recovery (IR) sequence (fit parameters from Figure 9), the zero-crossing (ZC) method, and the percent difference between the two methods.

The uncertainty range of the ZC method always encloses the value calculated from the IR value, as the uncertainty in the ZC method is highly inaccurate. However this does not hold true vice versa, as the uncertainty in the IR measurements is much lesser and does not encompass the ZC method values. For ethanol, as the time scales are much longer, it is difficult to generate an accurate estimation of where the zero-crossing point is – which is reflected in the percent difference from our more accurate IR method. The ZC method is a suitable procedure for estimating the T_1 constant, but as it is based off a single point, is not suitable for as a true measurement.

We may also compare this method to that used in Section 4.3. Comparing the values of T_1 using the IR method (Table 3) and the SR method (Table 2), the percent differences are 9.91% for doped water, 19.94% for ethanol, and 11.84% for rubber. While both the IR and SR methods have limitations and errors, the IR method is more accurate for calculating T_1 – as generating a fit over many data points reduces the propagation of random errors, which does not happen in Section 4.3 with the SR method. Thus, T_1 values calculated using the IR method, tabulated in Table 3, are considered as our most realistic time constants.

4.5 Hahn Echo

The raw data collected from the spectrometer was zero-shifted and smoothed using a simple Gaussian filtering procedure (see Appendix A). The peak magnetization of the echo decays as,

$$M(t) = M_0 e^{-t/T_2}$$

Similar to previous sections, taking the natural logarithm and rearranging,

$$\ln\left(M(t)\right) = \frac{-t}{T_2} + \ln(M_0) \tag{15}$$

Figure 10 shows each trace with different time-delays and the calculated echo amplitude. These amplitudes are plotted against $t = 2\tau$ in Figure 11, along with the fit – which was determined using a linear least squares regression of the data, using the form from Equation 15. From the fit, the T_2 value is the slope of the line, and the uncertainty is the 95% confidence interval of the least squares algorithm. The T_2 values for doped water, ethanol and rubber are summarized in Table 4.

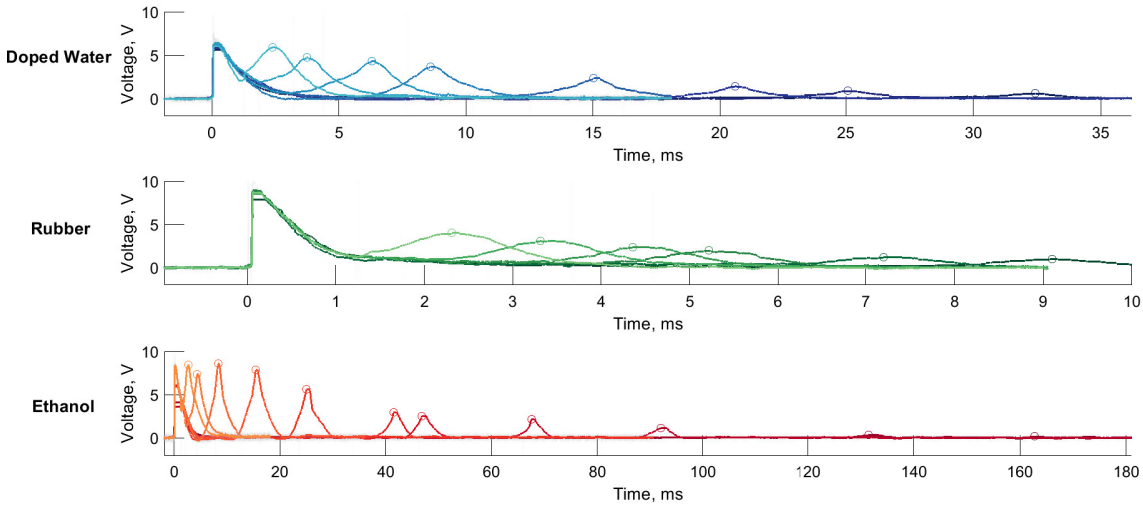

Figure 10: Time traces of Hahn echo experiments for the samples, with multiple traces for time-delay τ overlaid. The solid lines are the filtered data, light grey is the raw, unfiltered data, and the circle points are the calculated peak magnetization values at $t = 2\tau$.

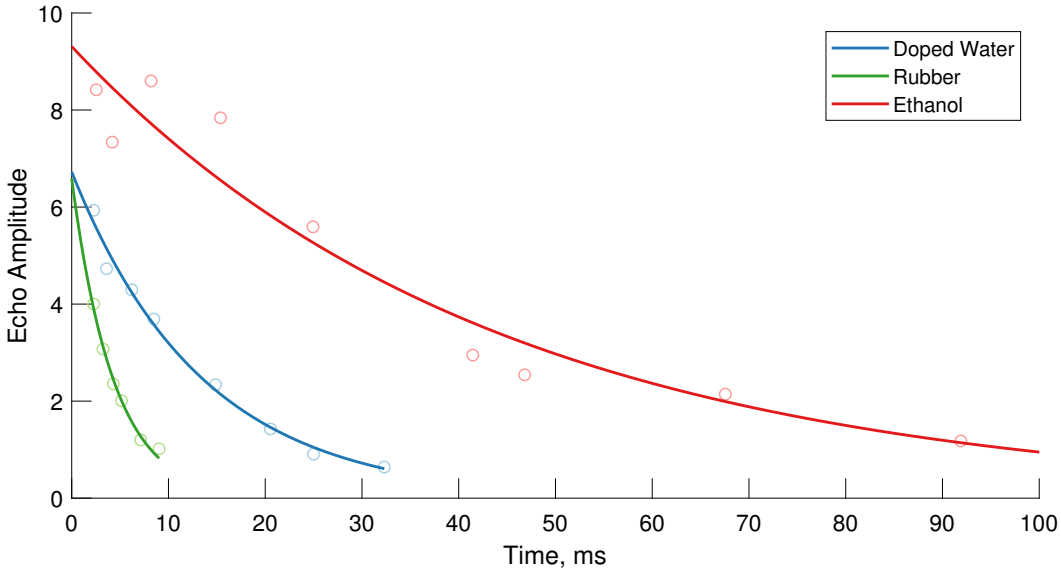

Figure 11: Peak magnetization of three samples, extracted from Figure 10 to determine T_2.

Sample	T_2 (ms)
Doped Water	13.31 ± 1.16
Ethanol	42.21 ± 3.38
Rubber	4.80 ± 1.11

Table 4: T_2 values for three samples determined using the Hahn echo experiments, calculated from the fit of results from Figure 11.

As expected from Equation 8,

$$1/T_2^* = 1/T_2 + \gamma \Delta B_o$$

all values of T_2 are greater than that of T_2^* (Table 1). Using these two terms, it is straightforward to calculate the $\gamma \Delta B_o$ values for each sample. As γ is constant for each sample (the gyromagnetic ratio of a proton) then from Table 5 we can compare the relative field inhomogeneities of each sample. We can see that rubber has greater field inhomogeneities than the liquid sample ethanol by a factor of approximately two. The rubber sample used here, a pencil eraser, likely has manufacturing impurities and spatial differences in density and chemical composition – compared to a highly pure sample of ethanol. Thus, it is consistent with our knowledge of the samples that the field inhomogeneities of rubber are greater than the other two samples.

Sample	$\gamma \Delta B_o$ (ms^{-1})
Doped Water	0.7876 ± 0.0126
Ethanol	1.0816 ± 0.0100
Rubber	2.1987 ± 0.0362

Table 5: Comparison of the field inhomogeneities for each sample, computed from the differences in T_2 (Section 4.4, IR method) and T_2^* (Section 4.2).

4.6 Freezing

This section of the experiment relied upon freezing our sample of doped water. Our graphs for the FID of ice vs water are shown in Figure 12. We clearly see that frozen water has no visible excitation.

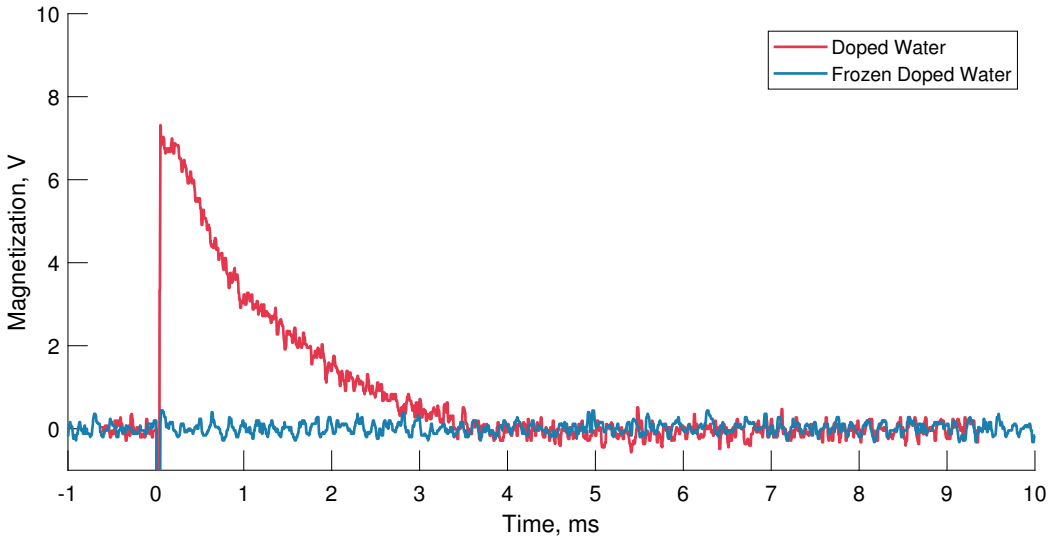

Figure 12: Example FID of doped water at room-temperature (liquid) and frozen (solid).

To explain this we note that in our derivation of $\vec{M}$, the magnetization vector, we assumed that each atom could rotate independently, which is true in a liquid, but is an untrue assumption when working with a solid. In a solid, orientation dependant effects are observed. Some examples of these effects are non-averaged dipolar interactions and chemical shift anistropy interactions. These non-averaged effects lead to the case where resonances are very broad.

To compare these liquid vs solid resonances it is typical to compare line width which is known to be < 1 Hz in liquid water while the resonances in ice is broadened up to ~10^5 Hz. [1] This means that a radio frequency signal to affect the magnetization would have to be broadband. To achieve a good signal the frequency needed to excite are generally around 50-100 kHz. [1].

In this experiment we excite with a single frequency, so due to this broad peak we are unable to resonate with a large amount of the atoms and hence we cannot change their orientation with the Rabi pulses, leading to a lack of signal.

Also, the spin lattice relaxation time (T_1) requires interactions with the external world, as it is due to thermal effects such as molecular rotation, diffusion, or lattice vibration [5], hence it can be very weak in the absence of molecular motion, as is in the case of low temperature crystalline structures such as frozen water. This means that the T_1 times of ice water are much larger than that of liquid waters. The ice water relaxation time has been measured to be 39.40s [7]. To gain a FID signal enough time must elapse between the successive pulses in order for the magnetization to build up along the z-axis so that the signal is large. Hence our repeat times which were 0.3s were such that the signal could not have been seen.

4.7 Comparison of Rubber and Ethanol

Here we briefly discuss some of the results and how they apply to the three samples. Note that the doped water is essentially a calibration sample as it has been modified to increase its signal. Hence we will investigate the differences between ethanol and rubber.

In analyzing these results, we can conclude that the time constants for ethanol are an order of magnitude larger than that of a rubber. The typical designation of "rubber" commonly refer to a class of polymers known as elastomers (although this is not completely accurate in specific cases [2]). These elastomers have high molecular mobility and narrow NMR lines due to their weak intermolecular forces between their polymer chains, [3]. These characteristics make them ideal for pulse NMR spectroscopy as the high molecular mobility has been linked to lower T_1 and T_2 times, which has been verified in references [4, 8]. This lowering of T_1 and T_2 based off of molecular mobility is due to the fact that interactions in general increase with an increase of molecular mobility. These interactions can be molecular collisions, which affect T_1 or higher fluctuations in local fields which affect T_2.

However in comparison the dominant intermolecular force present in ethanol is hydrogen bonding, which is a strong force, which directly leads to a decrease of molecular mobility and hence an increase in both T_1 and T_2.

5 Conclusion

In this experiment we explored the Nuclear Magnetic Resonance for three samples; a calibration sample of doped water, representative liquid sample of ethanol, and a representative solid sample of rubber. Using methods including free-induction decay, saturation-recovery, inversion-recovery and Hahn echo, the time constants T_1, T_2^* and T_2 are calculated for all three samples.

The ethanol sample has time constants $T_1 = 2357 \pm 82$ ms and $T_2 = 42.41 \pm 3.38$ ms, while rubber sample has constants $T_1 = 38.48 \pm 2.09$ ms and $T_2 = 4.80 \pm 1.11$ ms.

Using inversion-recovery sequence a more accurate method for calculating T_1 than the zero-crossing method or saturation-recovery method.

From the presented results, we can conclude that T_1 is approximately an order of magnitude larger than T_2 and the time constants for ethanol are an order of magnitude larger than that of a rubber due to the differences in inter-molecular forces.

Appendices

A Data Processing

All custom Matlab scripts for data processing are available on Github at `https://github.com/tokiyoshi/460_E20_NMR.git`.

In the data-processing, for each section the data was zero-shifted prior to any data fitting to account for any constant voltage offset from the spectrometer. For multiple sections, to extract values from the oscilloscope traces, smoothing was performed on the raw data to remove spurious noise and artifacts. In Sections 4.3, 4.4, and 4.5, automatic peak detection of the second pulse or Hahn echo was used – and it was necessary to perform filtering and thresholding of the data values to ensure proper peak detection. A Gaussian smoothing algorithm with window size dependent on the resolution of the oscilloscope trace was implemented, and if necessary, large peaks (such as large-voltage artifacts from cross-talk between the pulse and the detector) were removed via a simple voltage cutoff.

Other filtering algorithms were tested including Savitsky-Golay, median filter, and low-pass filters – however all introduced some artifacts (for example, low-pass filter removed the sharp increase of voltage due to a pulse and shifted the detected time of the pulse over) or did not improve the signal enough for further processing.

It is possible for the filtering to reduce the peak amplitude detected (this is most prevalent in Section 4.4), however the effects are minimal and as the value being calculated is the time-constant, we can assume that the filtering would only slightly change the initial magnetization amplitude, M_0 (as each peak is approximately reduced the same percentage), and not effecting the time constant. This effect is also present in Section 4.5, but when comparing the raw data to the filtered, there is negligible change in the amplitudes of the echos.

B Sources of Error

Unfortunately, throughout this lab there are effects seen throughout which strongly affect the signals which are being received. We will attempt to identify and describe them here, and state how attempts were made to mitigate the effects of these error sources if possible.

B.1 External Magnetic Effects / Drift

During the lab it is clear that the NMR spectrometer picks up small effects of external magnetic fields as the overall magnetization of the sample is due to the roughly 1 in 10^6 protons causing a small magnetic effect. We note that this magnetization will be heavily affected by small external effects. This is proven during the lab when a laptop was placed approximately 30 cm away from the sample, causing a complete deviation from resonance. During the lab any metal objects are moved away from the sample, but this source of error is difficult to eliminate completely. An example of this error comes from the drift of the paramagnet, caused by the magnet's thermal stabilization. Although the change in magnetization is known to be small due to thermal fluctuations, it is significant enough to be picked up and throughout the lab, this and other unknown effects necessitated that a re-calibration of inputted frequency signals to match resonance conditions.

B.2 Known Equipment Error

We also have seen that the spectrometer itself has components which cause an effect which can be seen, causing a "pulsing" of the signal. We were informed that this is a known issue, but means that data averaging would be inaccurate and we note that it is necessary to acquire single runs and visually inspect them. But this effect will cause some deviation from theory.

C Extra Plots

C.1 B2

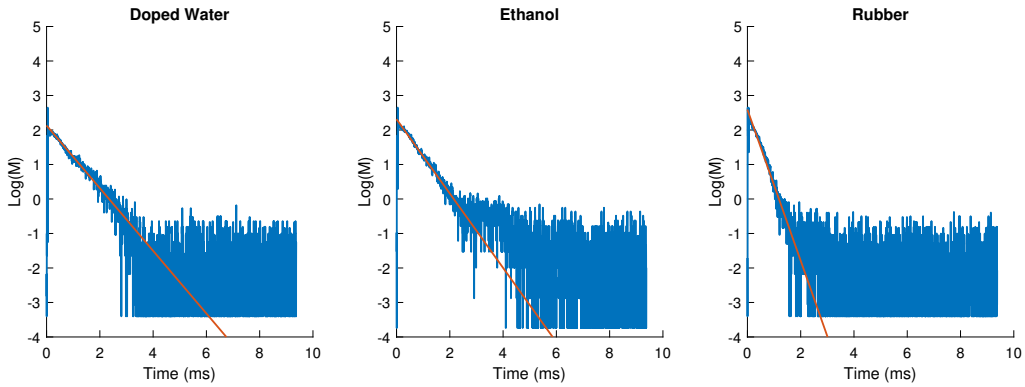

Figure 13: Linear fit to the logarithm of the magnetization for Section 4.2.

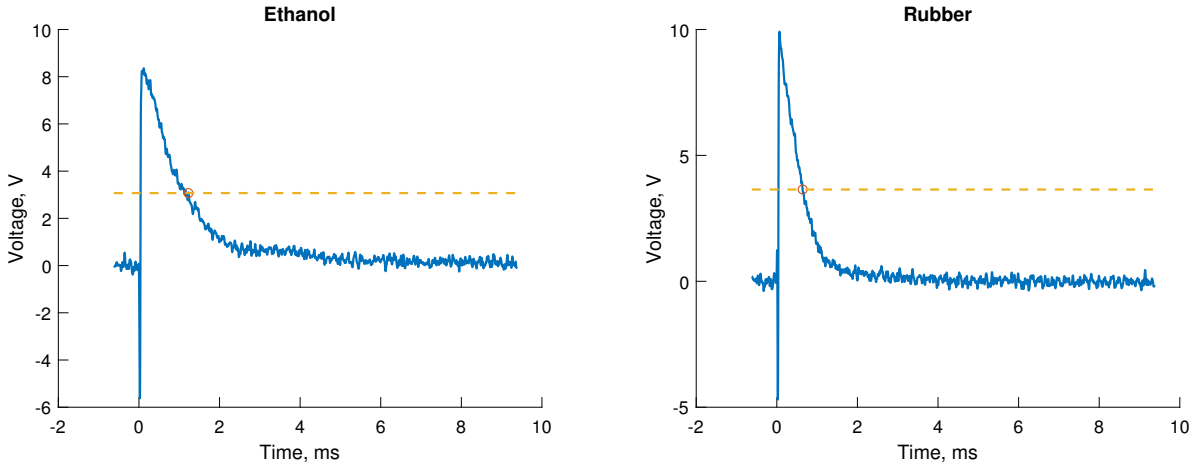

Figure 14: Plots of rubber and ethanol FID for estimation of T_2^* in Section 4.2.

References

[1] V. Bakhmutov, *NMR Spectroscopy in Liquids and Solids*, CRC Press, 2015.

[2] A. W. Birley, *Polymer science dictionary*, Polymer International, 24 (1991), pp. 127–127.

[3] B. Blumich and P. Blmler, *Nmr imaging of polymer materials*, Die Makromolekulare Chemie, 194 (1993), pp. 2133–2161.

[4] C. Chang and R. Komoroski, *Nmr imaging of elastomeric materials*, Macromolecules, 22 (1989), pp. 600–607.

[5] E. Fukushima and S. Roeder, *Experimental pulse NMR: A Nuts and Bolts approach*, The Advanced Book Program, Addison-Wesley Pub. Co., Advanced Book Program, 1981.

[6] E. L. Hahn, *Spin echoes*, Physical review, 80 (1950), p. 580.

[7] D. Le Botlan, J. Wennington, and J. Cheftel, *Study of the state of water and oil in frozen emulsions using time domain nmr*, Journal of colloid and interface science, 226 (2000), pp. 16–21.

[8] S. Stapf and S. Kariyo, *Dependence of order and dynamics in polymers and elastomers under deformation revealed by nmr techniques.*